An Adaptive droop Curve for the Superimposed Frequency Method in DC Microgrids

Jafari, Mohammad; Peyghami, Saeed; Mokhtari, Hossein; Blaabjerg, Frede

Published in:
Proceedings of the 2020 IEEE 21st Workshop on Control and Modeling for Power Electronics (COMPEL)

DOI (link to publication from Publisher):
10.1109/COMPEL49091.2020.9265777

Publication date:
2020

Document Version
Early version, also known as pre-print

An Adaptive droop Curve for the Superimposed Frequency Method in DC Microgrids

Mohammad Jafari Matehkolaei
The Center of Excellence in Power System Management and Control
Department of Electrical Engineering
Sharif University of Technology
Tehran, Iran
m.jfr.m74@gmail.com

Saeed Peyghami
Department of Energy Technology
Aalborg University
Aalborg, Denmark
sap@et.aau.dk

Hosein Mokhtari
The Center of Excellence in Power System Management and Control
Department of Electrical engineering
Sharif University of Technology
Tehran, Iran
mokhtari@sharif.edu

Frede Blaabjerg
Department of Energy Technology
Aalborg University
Aalborg, Denmark
fbl@at.aau.dk

***Abstract*— This paper proposes a new adaptive droop curve to ensure the stability of the superimposed frequency method (SFM) for the control of DC Microgrids. SFM has a remarkable accuracy in load-sharing and voltage regulations among different control strategies of DC microgrids. However, this method suffers from some levels of instability in terms of the load variations. This is due to (i) location of the system dominant poles; which is really sensitive to the variations of the system loading, and (ii) limitations in the transferred reactive power; which is used to regulate source DC voltages. Therefore, a new strategy based on an adaptive droop curve is presented in this paper to keep the system dominant poles in an acceptable area and its performance is verified using different simulation studies in MATLAB/SIMULINK environment.**

Keywords—DC Microgrids, Droop Curve, Load- Sharing, Voltage regulation, System dominant poles, Instability.

I. INTRODUCTION

Due to major global concerns about the global warming and imminent energy crisis, trends towards using distributed generations (DG) and renewable energy sources (RES) have increased recently [1]. However, direct integration of DGs and RESs to the conventional AC systems might cause severe problems for the system stability, protection, control, power quality, and etc. Microgrids are the base structures that are required for the large-scale application and integration of DGs and RES into the main AC systems [2].

There are two types of DC and AC microgrids. Due to the recent advances in power electronic converters, and introducing higher efficiency, reliability, controllability, DC microgrids are getting much popular than the past compared to its rival i.e. AC microgrids [2]. Furthermore, most of the loads and sources, like photovoltaic cells, energy storage systems (ESS) and most of DGs, have a DC nature or at least require AC/DC conversion in their structures.

Conventionally, DC microgrids are controlled in three stages of primary, secondary, and tertiary controllers. Droop curves are utilized in primary controllers to ensure the system stability and proper load-sharing. Voltage regulation of the system is ensured by the secondary controllers, and the tertiary controller is utilized for ensuring the optimal and economic operation of the system [1]. Conventional control methods of DC microgrids suffer from some major problems such as negative impact of line resistances on the equivalent droop curve, poor current sharing, and severe voltage drops. Furthermore, secondary controllers require a vast communication infrastructure that harshly affects the system reliability [2]-[6].

In [7], an adaptive droop curve is proposed for the primary controller which regulates droop gains according to the system overall loading. However, the overall load sharing is not desirable in this method. To enhance the overall load- sharing accuracy, a non-linear droop curve is introduced in [8]. However, this method increases the system overall complexity and controllability. To enhance system performance at the presence of constant power loads (CPL), a new droop curve based on the square of the DC bus voltage is presented in [9]. But, load- sharing accuracy and voltage regulation of the system are harshly affected. In [10], a master- slave based strategy is proposed to alleviate the problems caused by the primary controller. However, due to existence of only one master unit, this method does not yield an acceptable voltage regulation.

In order to solve all the aforementioned problems, a new strategy based on a superimposed AC voltage is proposed in [11]. The idea of the proposed method is mainly adopted from frequency droop in AC systems. In other words, each source injects a small AC voltage with a frequency related to its output DC current, and the system is stabilized using the sources frequency droop curve. The proposed superimposed frequency method in [11] has a desirable load-sharing and voltage regulation accuracy. Furthermore, this method does not require any communication infrastructures, and therefore, improves the system reliability. However, this method suffers from some levels of inaccuracy in terms of the load variations. This problem is mentioned in [12], [13], in which conventional droop curve is merged with the superimposed frequency droop method in order to solve the instability problem. However, the proposed method increases system complexity. In [14]- [16], adaptive droop curve and adaptive amplitude of the injected voltage is proposed to ensure system stability at different loadings. However, these methods also increase system complexity. Thus, this paper proposes a new adaptive droop curve to solve the instability problem of the superimposed frequency droop method. Furthermore, the proposed adaptive droop curve does not increase the system complexity, and does not require any communication infrastructure.

The paper is structured as follows. First, at section II, superimposed frequency droop method and some important factors are briefly discussed. Then, in section III, the proposed adaptive droop curve is introduced. Furthermore, performance of the proposed adaptive droop curve is investigated using small signal stability analysis and different simulation studies in section IV and V, respectively. Finally, section VI concludes the paper.

II. Reactive Power in SFM

The main purpose of the SFM is to adopt a new strategy for overcoming the inaccuracies in the conventional voltage-based control methods of DC microgrids. For this, a strategy mainly adopted from AC systems is used. In other words, a small AC signal is injected to the main DC system, and the system is controlled using the global frequency of this small AC signal. The main reason for the inaccuracies in the conventional voltage-based control methods is using the local parameter of voltage. Frequency droop method uses two types of droop curves i.e. frequency-DC current droop curve which is adopted from AC systems, and voltage-reactive power droop curve used for regulating the DC voltage of each source.

A. Frequency- DC current Droop Curve

In the SFM, a small AC voltage with a constant amplitude of A is injected to the main DC microgrid [11]. The frequency of the injected AC voltages is calculated using a frequency droop similar to the ones used in AC systems. At steady state, the systems frequency is stabilized and is calculated according to (1). The applied frequency droop is depicted in Fig. 1(a).

$$f = f^{*} - d_{fi} I_i \,, \; i = 1,2,\ldots,N \tag{1}$$

where N is the number of DGs in the microgrid, f is the system frequency, f^* is the system reference frequency, d_{fi} is the frequency droop gain of i^{th} source, and I_i is the DC current of the i^{th} source.

B. Voltage- Reactive power Droop curve

Schematic of the applied voltage droop curve is depicted in Fig. 1(b). In the SFM, the DC voltage of each source is regulated using a voltage-reactive power droop curve as [11]:

$$V_i = V_{ref} - d_i Q_i \,; \quad i = 1,2 \tag{2}$$

where d_i is the voltage droop gain of i^{th} source, Q_i is the injected reactive power of the i^{th} source, V_i is the output DC voltage of the i^{th} source, and V_{ref} is the reference DC voltage of the microgrid.

The value of the voltage droop gains, i.e. d_i, has a fundamental impact on the transferred reactive power among the sources. For analyzing this, a simple DC microgrid with the configuration of Fig. 2 and a local resistive load is considered. For this grid, a local resistive load is considered. For the system in Fig. 2, DC voltage of the i^{th} source is calculated as:

$$V_i = V_{PCC} + r_i I_i \,; \; i = 1,2$$
$$V_{PCC} = R_{load}(I_1 + I_2) \tag{3}$$

where V_{PCC} is the voltage of the PCC, R_{load} is the load resistance, and r_1, r_2 are the line resistances of the sources 1 and 2.

According to [12], the required transferred reactive power among the two sources and the maximum transferrable reactive power is as (4).

$$Q = \frac{V_{ref}(d_{f1} r_2 - d_{f2} r_1)}{R_{load}(d_1 + d_2)(d_{f1} + d_{f2}) + r_1 d_2 d_{f2} + r_2 d_1 d_{f1}} \;;$$
$$Q_{\max} = \frac{A^2}{2(r_1 + r_2)} \tag{4}$$

where R_{load} is the load resistance, and r_1, r_2 are the line resistances of the sources 1 and 2.

Using (4), for the system shown in Fig. 2, the effect of the voltage droop gain in the maximum loading of the system is depicted in Fig. 3. As shown in this figure, using higher/lower voltage droop gains, the system maximum loading is increased/decreased. In order to further analyze the effect of the voltage droop gains, variations of the transferred reactive power among the two sources in terms of the variations in voltage droop gains at a constant loading is depicted in Fig. 4. As shown in this figure, the values of voltage droop gains have an influential impact on the transferred reactive power. At first sight, it might look reasonable to use high droop gains. However, high droop gains decrease the system damping ratio, and might lead to system instability. This matter is further investigated in section 4. In other words, using constant voltage droop gains, only a limited range of the loads can be supplied by the system. Therefore, it is desirable to have high/low droop gains at high/low loadings.

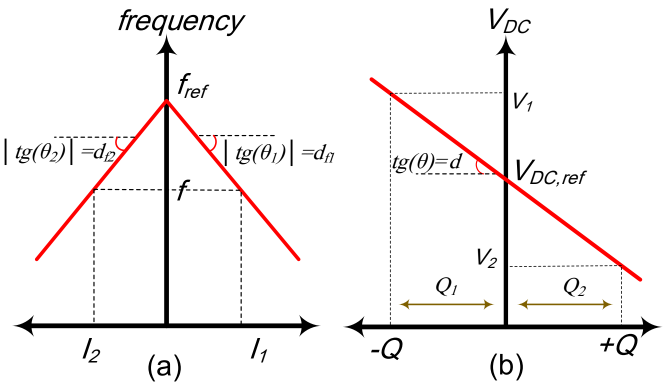

Fig. 1. Schematics of (a) Frequency- DC current droop curve (b) Voltage-Reactive power droop curve [11]

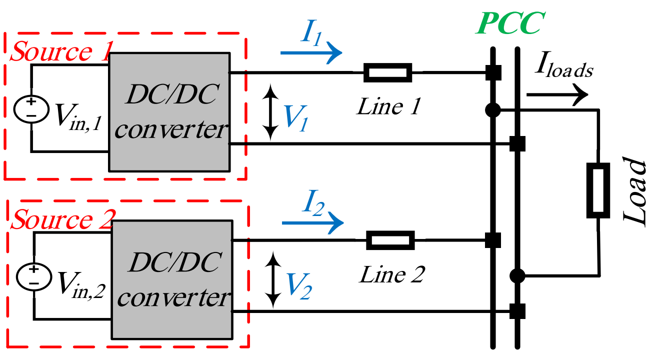

Fig. 2. Schematics of a typical DC microgrid *($r_1 = 2\Omega$, $r_2 = 4\Omega$, $V_{DC,ref} = 700V$, $d_{f1} = d_{f2} = 0.15$, $A = 10V$)* [11]

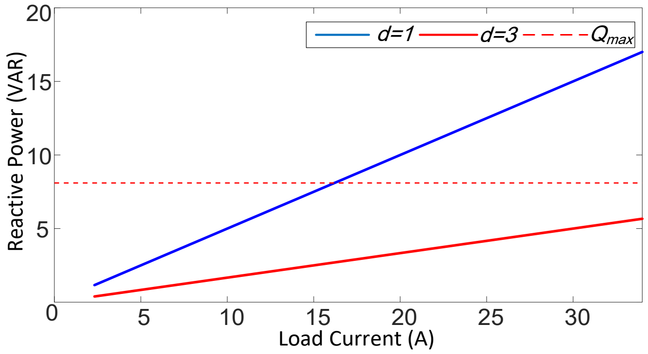

Fig. 3. Impact of voltage droop gains on transferred reactive power among the sources with contant voltage droop gains [14]- [16]

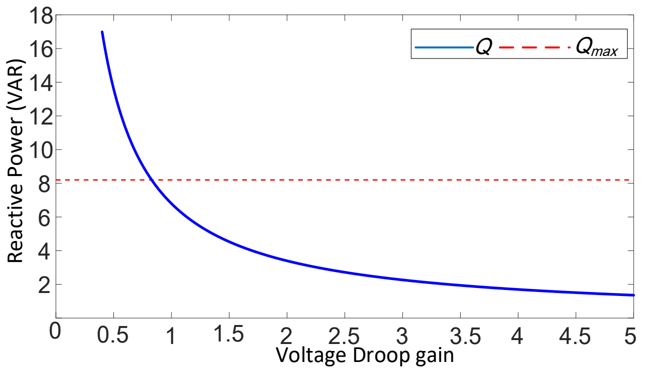

Fig. 4. Impact of voltage droop gains on transferred reactive power among the sources at constant loading ($1 < d < 6$, $R_{load} = 50\ \Omega$) [14]- [16]

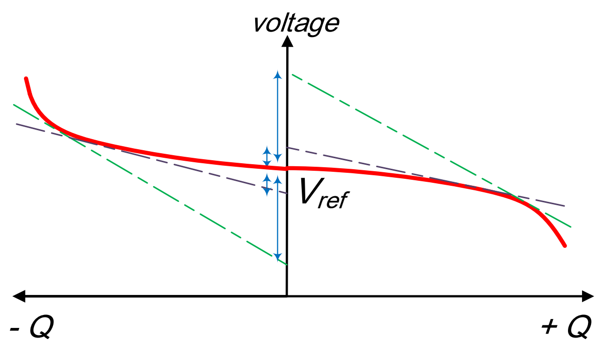

Fig. 5. Schematics of the proposed adaptive droop curve

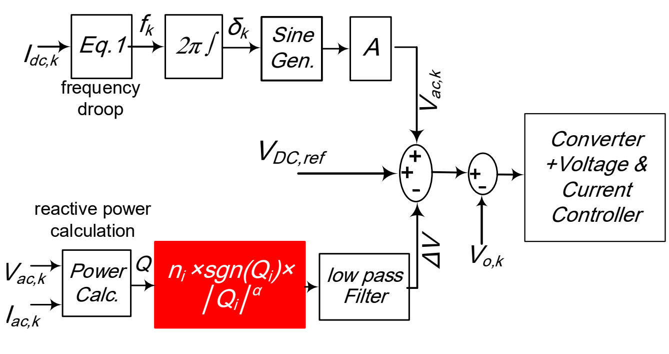

Fig. 6. Schematics of control block diagram of the sources using the proposed adaptive droop curve

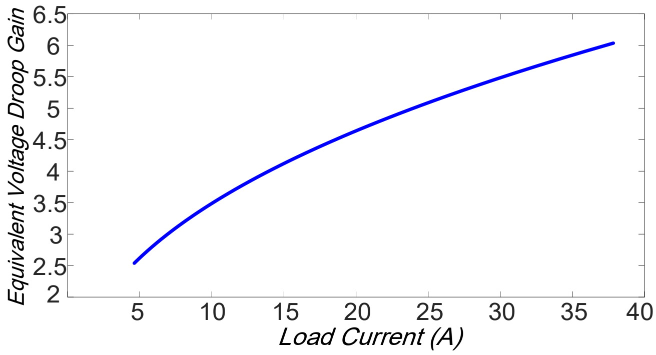

Fig. 7. Variation of the voltage droop gain in terms of the load variations for the proposed adaptive droop curve

III. The Proposed Adaptive Droop Curve

As discussed in the former section, it is desirable to have high/low voltage droop gains at high/low loading of the system. In the other words, the system voltage droop gains must be proportional to the overall loading of the system and change according to it. As shown in Fig. 3 and Fig. 4, the transferred reactive power among the two sources increases as the system loading increases. Therefore, the transferred reactive power can be set as a criterion for determining the overall load of the system and changing the voltage droop gains. Schematic of the proposed adaptive droop curve is depicted in Fig. 5, and the sources control block diagram is depicted in Fig. 6. In the proposed droop curve, the voltage of each sources is calculated as:

$$V_i = V_{ref} - sgn(Q_i) n_i |Q_i|^{\alpha} \quad ; \qquad \mathrm{sgn}(x) = \begin{cases} 1 & ; x \geq 0 \\ -1 & ; x < 0 \end{cases} \tag{5}$$

where $sgn(x)$ is the sign function, and n_i and α are the proposed droop curve constant and coefficient.

The voltage droop gain at each operating point of the system can be calculated as (6). Using (6), for the system in Fig. 2, variations of the source voltage droop gains in terms of load variations is depicted in Fig. 7. As depicted in Fig. 7, voltage droop gains are set according to the overall loading of the system and will increase/decrease as the system loading increases/decreases. Therefore, using the proposed adaptive droop curve, variations of the voltage droop gains will be desirable, and will enhance the system performance.

$$d_{i0} = \left| \frac{\partial V_i}{\partial Q_i} \right| = n_i \alpha |Q_{i0}|^{\alpha - 1} \tag{6}$$

With refer to [11], for the acceptable operation of the system, it is better that the transferred reactive power remain in the range of 20% and 80% of the maximum transferrable reactive power at all loadings of the system. Because, very low amount of the transferred reactive power can cause some problems in the detection of the small AC current, and very high value of the transferred reactive power can lead to system instability. This is further explained in section 4. Therefore, d_{min} must be imposed at the lowest load (with $0.2Q_{max}$), and d_{max} must be imposed the highest loading (with $0.8Q_{max}$). Therefore, using the equations in (7), the value of α can be calculated. By substituting the value of α in any of the equations in (7), the value of n_i can be calculated.

$$\begin{cases} d_{\min} = n\alpha(0.2Q_{\max})^{\alpha-1} \\ d_{\max} = n\alpha(0.8Q_{\max})^{\alpha-1} \end{cases} \tag{7}$$
$$\Rightarrow \quad \alpha = 1 + \log_4 \frac{d_{\max}}{d_{\min}}$$

IV. Small Signal Stability Analysis

After Dynamic behavior of the SFM using the proposed adaptive droop curve for the system in Fig. 2 is investigated in this section. The linear model of (5) and (6) are presented in (10) and (11), respectively.

$$\begin{cases} \Delta Q_1 = -k_\delta \Delta\delta \\ \Delta Q_2 = k_\delta \Delta\delta \end{cases} ;$$
$$k_\delta = \frac{A^2}{2(r_1 + r_2)} \cos\delta_0 \tag{8}$$

$$\begin{cases} \Delta V_1 = -n\alpha |Q_1|^{\alpha-1} G_{(s)} \Delta Q_1 \\ \Delta V_2 = -n\alpha |Q_2|^{\alpha-1} G_{(s)} \Delta Q_2 \end{cases} \tag{9}$$

where $G_{(S)} = w_c / (S + w_c)$ is a low pass filter with the cutoff frequency of w_c, and S is the Laplace operator.

By substituting the values of ΔQ_1 and ΔQ_2 into (9), and merging the equivalent equation with the small signal model of (3), the linear model of I_1 and I_2 can be calculated as:

$$\begin{cases} \Delta I_1 = \frac{1}{h} k_\delta R_{load}\, n \left[|Q_1|^{\alpha-1} \times \frac{r_2 + R_{load}}{R_{load}} + |Q_2|^{\alpha-1} \right] G_{(s)} \Delta\delta \\ \Delta I_2 = -\frac{1}{h} k_\delta R_{load}\, n \left[|Q_1|^{\alpha-1} + |Q_2|^{\alpha-1} \times \frac{r_1 + R_{load}}{R_{load}} \right] G_{(s)} \Delta\delta \end{cases} ;$$
$$h = r_1 r_2 + R_{load}(r_1 + r_2)\,. \tag{10}$$

According to [11], δ can be calculated as:

$$\delta = \frac{2\pi}{S}(d_{f2} I_2 - d_{f1} I_1) \tag{11}$$

By substituting ΔI1 and ΔI2 from (10) into the linear model of (11), characteristic equation of the system is calculated as (12).

$$S^2 + w_c S + \frac{\beta}{h} = 0 \tag{12}$$

$$\beta = 2\pi R_{load}\, n\alpha k_\delta w_c \left[\begin{array}{l} d_{f1}\left(|Q_1|^{\alpha-1} \times \frac{r_2 + R_{load}}{R_{load}} + |Q_2|^{\alpha-1} \right) \\ + d_{f2}\left(|Q_1|^{\alpha-1} + |Q_2|^{\alpha-1} \times \frac{r_1 + R_{load}}{R_{load}} \right) \end{array} \right] ;$$
$$h = r_1 r_2 + R_{load}(r_1 + r_2)\,. \tag{13}$$

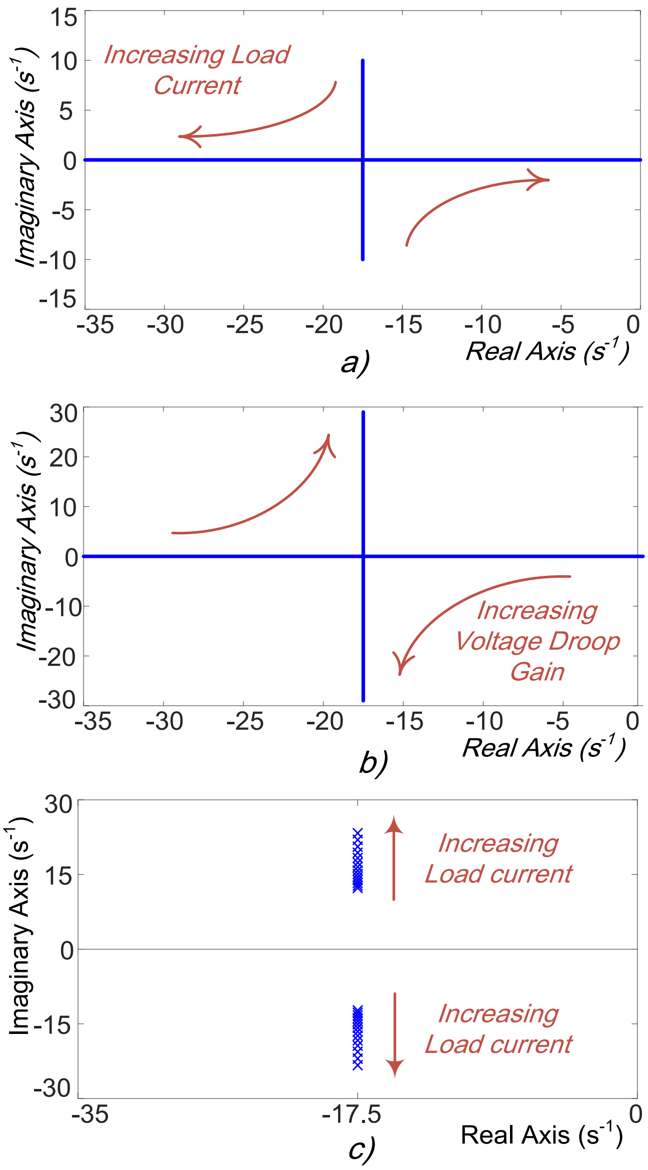

Fig. 8. Root locus of the system (a) the impact of increasing load with constnt droop gain ($d = 2$, $20 < R_{load} < 150\ \Omega$) (b) the impact of increasing voltage groop gain at a constant load ($1 < d < 6$, $R_{load} = 50\ \Omega$) (c) the proposed adaptive droop curve ($n_i = 1.1$, $\alpha = 1.7$, $20 < R_{load} < 200\ \Omega$)

At first, for the system in Fig. 2, using the conventional constant droop gain i.e. α=1, root locus of the system is depicted in Fig. 8(a). As shown in this figure, the system poles move towards the imaginary axis as the system loading increases. This will lead to the system instability at high loadings. At low loadings, the imaginary part of the system loading is so high, which leads to low damping ratio and system instability at low loadings. At a constant load, the effect of the voltage droop gains on the location of the system dominant poles is depicted in Fig. 8(b). As shown in this figure, voltage droop gains have an influential impact on the system stability. High voltage droop gains decrease the system damping ratio and might lead to system instability at low loadings. However, the system performance will be so desirable at high loadings. Low voltage droop gains might cause instability at high loadings. However, the system performance would be acceptable at low loadings. Therefore, high/low voltage droop gains are desirable for high/low loadings of the system. Using the proposed adaptive droop curve, root locus for the system in Fig. 2 is depicted in Fig. 8(c). As shown in this figure, the imaginary part of the system poles is low at low loads, and the system damping ratio is high. At high loadings, the system poles move away from the imaginary axis which guarantees system stable operation. Using the proposed adaptive droop curve, system poles remain in an acceptable area at all loadings of the system. Therefore, much wider range of the loads can be supplied by the system.

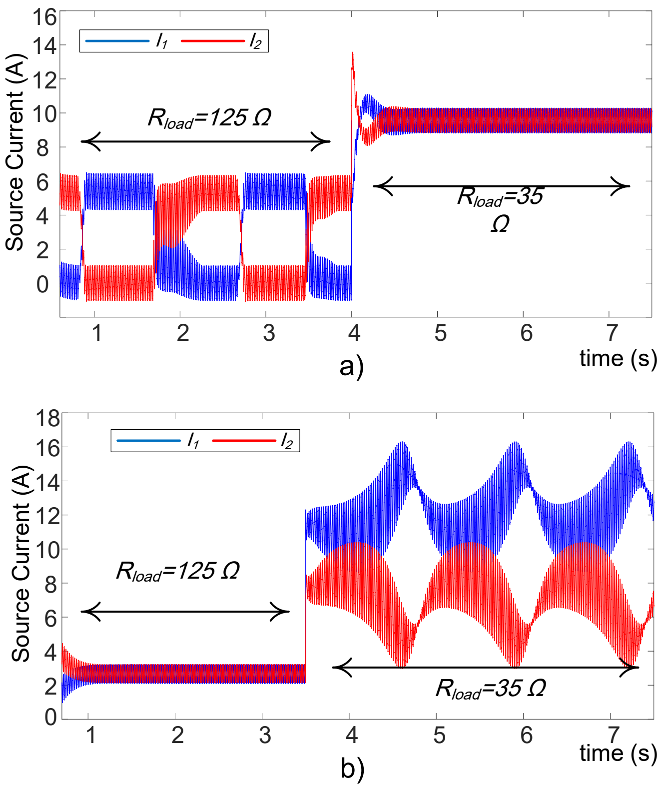

Fig. 9. Performance of the SFM at (a) high voltage droop gains *(d=3)* (b) low voltage droop gains *(d=1)*

V. Simulations

Simulation results for verifying the performance of the proposed adaptive droop curve is provided in this section. At first, the system in Fig. 2 is simulated with high voltage droop gain, and the results are presented in Fig. 9(a). As shown in this figure, the system performance is perfect at high loading. However, the system does not operate accurately at low loading. The system simulation results with low voltage droop gain are provided in Fig. 9(b). As shown in this figure, the system stability is desirable at low loading. However, its performance is not acceptable as the load increases.

Simulation results of the proposed adaptive droop curve are provided in Fig. 10. In Fig. 10(a), output currents of the sources are depicted. As shown in this figure, the system works perfectly at all loadings of the system, current-sharing accuracy is so desirable, and the load current is equally supplied by the two sources. The frequency of the injected AC voltage is depicted in Fig. 10(b). As shown in this figure, the two frequencies merge to a constant value at all loadings of the system, which attests the stable operation of the system using the proposed adaptive droop curve at different loadings of the system. The voltage of the two sources and their average value are depicted in Fig. 10(c). As shown in this figure, the average voltage of the buses is equal to the microgrid reference voltage at all loadings of the system. This is a testimony to the desirable voltage regulation of the SFM using the proposed adaptive droop curve. Therefore, using the proposed adaptive droop curve for SFM, the system performance will be desirable at all loadings of the system and the system load- sharing accuracy, voltage regulation, and stability is acceptable.

VI. Conclusion

This paper proposes a new adaptive droop curve in order to ensure the stability of the superimposed frequency droop method at all loadings of the system. In the proposed droop curve, droop gains are regulated regarding the overall loading of the system. Changing the droop gains will keep the system dominant poles in an acceptable area in order to ensure the stability of the superimposed frequency droop method at all loadings of the system. Performance of the proposed droop curve is validated using different simulation studies in MATLAB/SIMULINK environment.

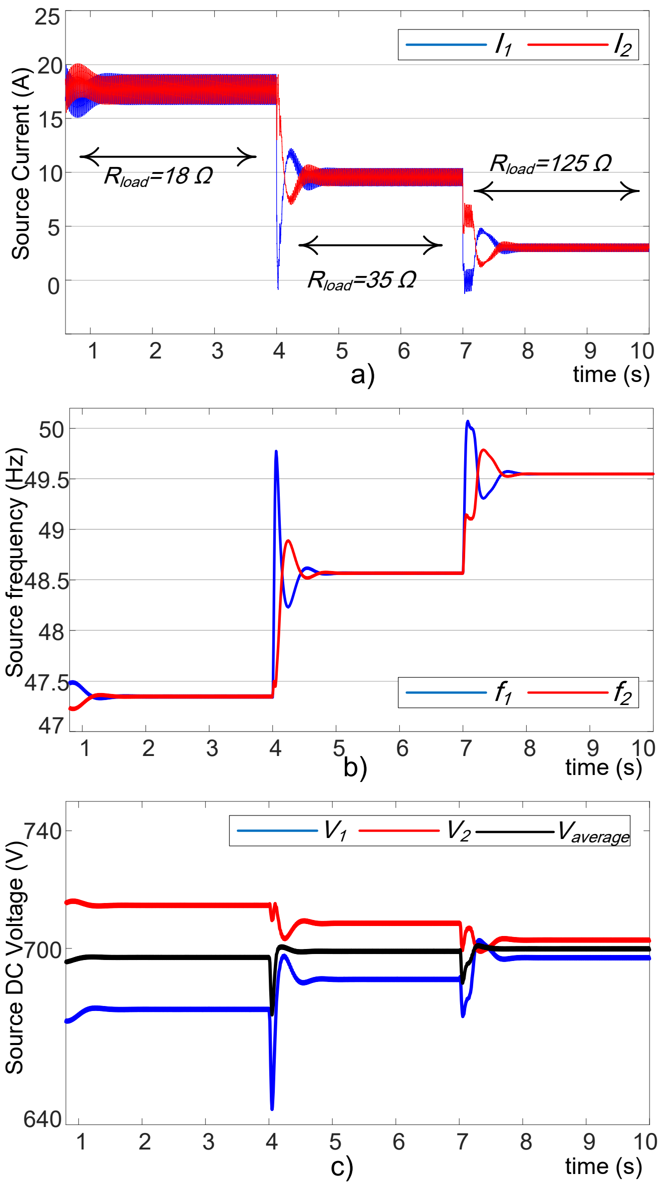

Fig. 10. Performance of the SFM with the proposed adaptive droop curve *(n_i=1.1, α=1.7)* (a) source output currents (b) frequency of the injected AC voltage (d) DC voltage of the sources

References

[1] H. Minxiao, S. Xiaoling, L. Shaobo and Z. Zhengkui, "Transient analysis and control for microgrid stability controller," *2013 IEEE Grenoble Conference*, Grenoble, 2013, pp. 1-6, doi: 10.1109/PTC.2013.6652175.

[2] M. R. Hossain and H. L. Ginn, “Real-Time Distributed Coordination of Power Electronic Converters in a DC Shipboard Distribution System,” *IEEE Trans. Energy Convers*., vol. 32, no. 2, pp. 770–778, Jun. 2017.

[3] D. Chen, L. Xu and L. Yao, "DC Voltage Variation Based AutonomousControl of DC Microgrids," *IEEE Trans. Power Deliv*., vol. 28, no. 2, pp. 637-648, April 2013.

[4] S. Anand, B. G. Fernandes, and J. M. Guerrero, “Distributed Control to Ensure Proportional Load Sharing and Improve Voltage Regulation in Low-Voltage DC Microgrids,” *IEEE Trans. Power Electron.*, vol. 28, no. 4, pp. 1900–1913, 2013.

[5] V. Nasirian, A. Davoudi, F. L. Lewis, and J. M. Guerrero, “Distributed Adaptive Droop Control for Dc Distribution Systems,” *IEEE Trans. Energy Convers*., vol. 29, no. 4, pp. 944–956, 2014.

[6] K. Sun, L. Zhang, Y. Xing and J. M. Guerrero, "A Distributed Control Strategy Based on DC Bus Signaling for Modular Photovoltaic Generation Systems With Battery Energy Storage," *IEEE Trans. Power Electron.*, vol. 26, no. 10, pp. 3032-3045, Oct. 2011, doi: 10.1109/TPEL.2011.2127488.

[7] Amir Khorsandi, Mojtaba Ashourloo, Hossein Mokhtari, Reza Iravani, “Automatic droop control for a low voltage DC microgrid, ” *IET Gener. Transm. Distrib*., vol. 10, Iss. 1, pp. 41–47, 2016, doi: 10.1049/iet-gtd.2014.1228.

[8] P. Prabhakaran, Y. Goyal and V. Agarwal, "Novel Nonlinear Droop Control Techniques to Overcome the Load Sharing and Voltage Regulation Issues in DC Microgrid," *IEEE Trans. Power Electron*., vol. 33, no. 5, pp. 4477-4487, May 2018.

[9] Y. Xia, W. Wei, Y. Peng, P. Yang and M. Yu, "Decentralized Coordination Control for Parallel Bidirectional Power Converters in a Grid-Connected DC Microgrid," *IEEE Trans. Smart Grid*, vol. 9, no. 6, pp. 6850-6861, Nov. 2018.

[10] Y. Gu, W. Li and X. He, "Frequency-Coordinating Virtual Impedance for Autonomous Power Management of DC Microgrid," *IEEE Trans. Power Electron.*, vol. 30, no. 4, pp. 2328-2337, April 2015, doi: 10.1109/TPEL.2014.2325856.

[11] R. Han, M. Tucci, A. Martinelli, J. M. Guerrero and G. Ferrari-Trecate, "Stability Analysis of Primary Plug-and-Play and Secondary LeaderBased Controllers for DC Microgrid Clusters," *IEEE Trans. Power Syst.*, vol. 34, no. 3, pp. 1780-1800, May 2019.

[12] S. Peyghami, H. Mokhtari, and F. Blaabjerg, " Autonomous Power Management in LVDC Microgrids based on a Superimposed Frequency Droop," *IEEE Trans. Power Electron*., vol. 33, no. 6, June 2018.

[13] S. Peyghami, H. Mokhtari and F. Blaabjerg, "Decentralized Load Sharing in a Low-Voltage Direct Current Microgrid With an Adaptive Droop Approach Based on a Superimposed Frequency," *IEEE J. of Emerg. Sel. Top. Power Electron.*, vol. 5, no. 3, pp. 1205-1215, Sept. 2017, doi: 10.1109/JESTPE.2017.2674300.

[14] M. Jafari, S. Peyghami, H. Mokhtari and F. Blaabjerg, "Enhanced Frequency Droop Method for Decentralized Power Sharing Control in DC Microgrids," *IEEE J. Emerg. Sel. Top. Power Electron.*, doi: 10.1109/JESTPE.2020.2969144.

[15] M. J. Matehkolaei and H. Mokhtari, "A Superimposed Frequency Method with an Adaptive Droop Characteristic for DC Microgrids," *2019 International Aegean Conference on Electrical Machines and Power Electronics (ACEMP) & 2019 International Conference on Optimization of Electrical and Electronic Equipment (OPTIM)*, Istanbul, Turkey, 2019, pp. 447-452, doi: 10.1109/ACEMP-OPTIM44294.2019.9007137.

[16] M. J. Matehkolaei, H. Mokhtari and M. Poshtan, "Automatic Superimposed Droop Frequency Control Scheme for DC Microgrids," *2019 International Aegean Conference on Electrical Machines and Power Electronics (ACEMP) & 2019 International Conference on Optimization of Electrical and Electronic Equipment (OPTIM)*, Istanbul, Turkey, 2019, pp. 120-125, doi: 10.1109/ACEMP-OPTIM44294.2019.9007132.